

## Analysis of end-plate connections at elevated temperatures

Shuyuan Lin<sup>\*</sup>, Zhaohui Huang<sup>a</sup> and Mizi Fan<sup>b</sup>

*School of Engineering and Design, Brunel University, Uxbridge, Middlesex, UB8 3PH, UK*

*(Received May 17, 2012, Revised December 14, 2012, Accepted June 04, 2013)*

**Abstract.** In this paper a robust 2-noded connection element has been developed for modelling the bolted end-plate connection between steel beam and column at elevated temperatures. The numerical procedure described is based on the model proposed by Huang (2011), incorporating additional developments to more precisely determinate the tension, compression and bending moment capacities of end-plate connection in fire. The proper failure criteria are proposed to calculate the tension capacity for each individual bolt row. In this new model the connection failure due to bending, axial tension, compression and shear are considered. The influence of the axial force of the connected beam on the connection is also taken into account. This new model has the advantages of both the simple and component-based models. In order to validate the model a total of 22 tests are used. It is evident that this new connection model has ability to accurately predict the behaviour of the end-plate connection at elevated temperatures, and can be used to represent the end-plate connections in supporting performance-based fire resistance design of steel-framed composite buildings.

**Keywords:** end-plate connection; component-based model; fire resistance; steel structures; T-stub

---

### 1. Introduction

In the last two decades significant progress has been made on the understanding of steel-framed composite buildings under fire conditions. Current research indicates that the robustness of steel connections is vitally important to the fire resistance of composite buildings. In recent years, an increasing number of investigations on the behaviour of steel connections have been conducted by different researchers. For example, Lawson (1990) carried a series of experiments to test the behaviour of steel joints at elevated temperatures. Leston-Jones (1997) conducted the experiments on flush end-plate connections in fire, followed by the tests on flexible endplate connections conducted by Al-Jabri *et al.* (2005). Structural engineers believe that for performance-based structural fire engineering design the steel connections should be simulated using 3D structural global modelling.

For modelling the behaviour of beam-to-column connections at elevated temperatures, three main approaches have been adopted in the past:

- (1) to represent the moment–rotation characteristics of a connection by mathematical

---

<sup>\*</sup>Corresponding author, Ph.D. Student, E-mail: [Shuyuan.Lin@brunel.ac.uk](mailto:Shuyuan.Lin@brunel.ac.uk)

<sup>a</sup> Reader, E-mail: [Zhaohui.Huang@brunel.ac.uk](mailto:Zhaohui.Huang@brunel.ac.uk)

<sup>b</sup> Professor, E-mail: [Mizi.Fan@brunel.ac.uk](mailto:Mizi.Fan@brunel.ac.uk)

expressions (in the form of curve-fitting equations), based on moment–rotation–temperature data obtained from experimental fire tests (Al-Jabri 1999);

(2) to use component-based (also known as spring-stiffness) models for predicting the behaviour of the connection. The methods are based on dividing the connection into its basic components, such as end plate, column flange, bolts, etc., and each component is idealized as a spring. The behaviour of the connection can be determined by assembling the stiffnesses of individual components to obtain the global stiffness of the connection (Ramli Sulong *et al.* 2010);

(3) to model the connection as assembly of 3D finite shell, brick and contact elements in which both geometrical and material nonlinearities are considered (Qian *et al.* 2009).

The first method is simpler, however the mathematical representation of the moment-rotation curve is generated from experimental test data. Hence, the model is limited to the joints which are similar to those previously investigated experimentally. In this simplified model the influence of the axial force of beam on the connection is also not accounted for. The third method can be attempted using general commercial software, such as ABAQUS or ANSYS. However this approach is computationally expensive, making it difficult to scale-up this approach for the analysis of complex global structures or sub-structures.

The second component-based modelling approach is now becoming popular for modelling the responses of connections subject to fire attack. This modelling approach is based on the experimental and analytical work conducted by Zoetemeijer (1974). The basic idea is to separate the connection into a series of springs. Each spring, regarded as an individual basic component, has its own strength and stiffness characteristics in tension, compression or shear. The overall behaviour of the connection can be then represented by the combination of these springs. As

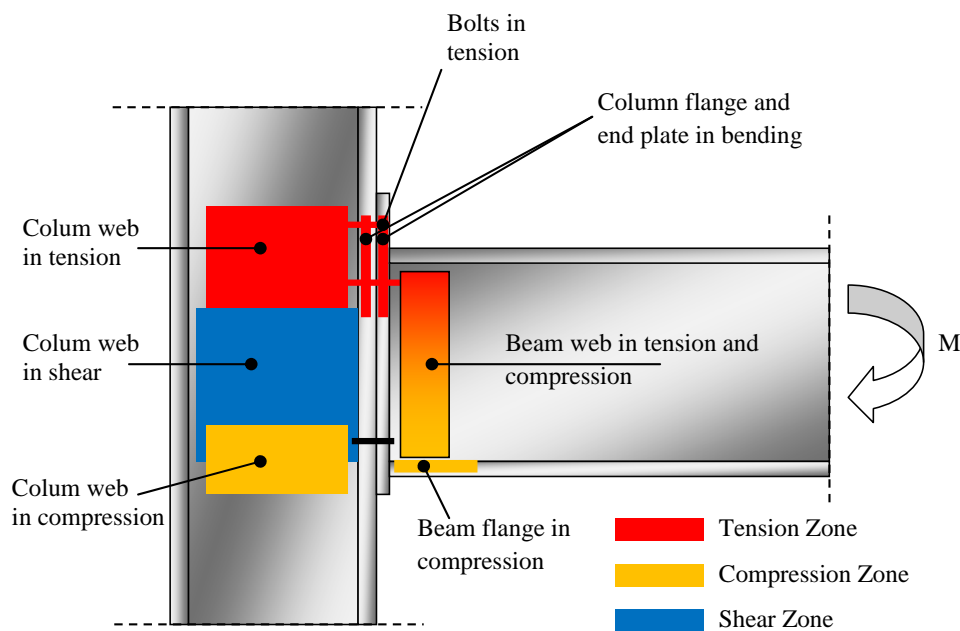


Fig. 1 Components within a bolted end-plate joint

shown in Fig. 1, for a bolted end-plate connection the main components are classified as column web in tension, bolts in tension, column flange and end-plate in bending, beam web in tension and compression, column web in compression, beam flange in compression, and column web in shear. However, the major shortcoming of component-based model is that under a static solver the analysis may terminate if the first component of the connection fails due to numerical singularity. A dynamic solver is needed to overcome this problem, which significantly reduces the computational efficiency of the approach.

Recently, Huang (2011) has developed a robust 2-noded connection element for modelling the bolted end-plate connection between steel beam and column at elevated temperatures. The model represents the connection as a 2-noded nonlinear spring. The characteristics of the spring, such as stiffness, the resistances of tension, compression and shear, bending moment resistance, are calculated based on the individual components of the connections. In Huang's model the characteristic of each component is determined by using the formulas proposed in Eurocode 3 Part 1.8 (2005b), and extended specifically for modelling fire by considering material properties as temperature dependent. This model has been found to be on the conservative side compared with test results. However, Huang's model combines the advantages of both the simplified and component-based models.

The main objective of this paper is to develop robust models for predicting the tension capacity of each individual bolt row and compression resistances of end-plate connections. The models are based on a component-based approach with robust deformation criteria of a T-stub. In the models the three failure modes of a T-stub have been taken into account. These new developments are incorporated into Huang's 2-noded end-plate connection model (Huang 2011). Through this integration the model developed in this paper also retains the advantages of both the simplified and component-based models.

## 2. Development of the numerical procedure

The proposed numerical procedure is based on a modification of the two-noded connection element developed by Huang (2011). In his original model, the connection is regarded as a two-noded element which has no physical length (see Fig. 2). Each node has six degrees of freedom: three translational degrees of freedom  $u$ ,  $v$ ,  $w$ , and three rotational degrees of freedom  $\theta_x$ ,  $\theta_y$ ,  $\theta_z$ , where  $x$ ,  $y$ ,  $z$  are local coordinates of steel beam element in which  $x$  is the direction of longitudinal axis of the beam element. Hence, the relationship of the nodal force increment vector  $\Delta \mathbf{F}$  and the nodal displacement increment vector  $\Delta \mathbf{u}$  can be given as

$$\Delta \mathbf{F} = \mathbf{K} \Delta \mathbf{u} \quad (1)$$

where  $\mathbf{K}$  is the stiffness matrix of connection element.

The nodal increment vectors  $\Delta \mathbf{F}$  and  $\Delta \mathbf{u}$  for the two-noded connection element are represented as

$$\Delta \mathbf{F}^T = \left[ \Delta F_{x,1} \ \Delta F_{y,1} \ \Delta F_{z,1} \ \Delta M_{x,1} \ \Delta M_{y,1} \ \Delta M_{z,1} \ \Delta F_{x,2} \ \Delta F_{y,2} \ \Delta F_{z,2} \ \Delta M_{x,2} \ \Delta M_{y,2} \ \Delta M_{z,2} \right] \quad (2)$$

$$\Delta \mathbf{u}^T = \left[ \Delta u_1 \ \Delta v_1 \ \Delta w_1 \ \Delta \theta_{x,1} \ \Delta \theta_{y,1} \ \Delta \theta_{z,1} \ \Delta u_2 \ \Delta v_2 \ \Delta w_2 \ \Delta \theta_{x,2} \ \Delta \theta_{y,2} \ \Delta \theta_{z,2} \right] \quad (3)$$

The element stiffness matrix  $\mathbf{K}$  is a  $12 \times 12$  matrix and defined by Huang (2011). There are

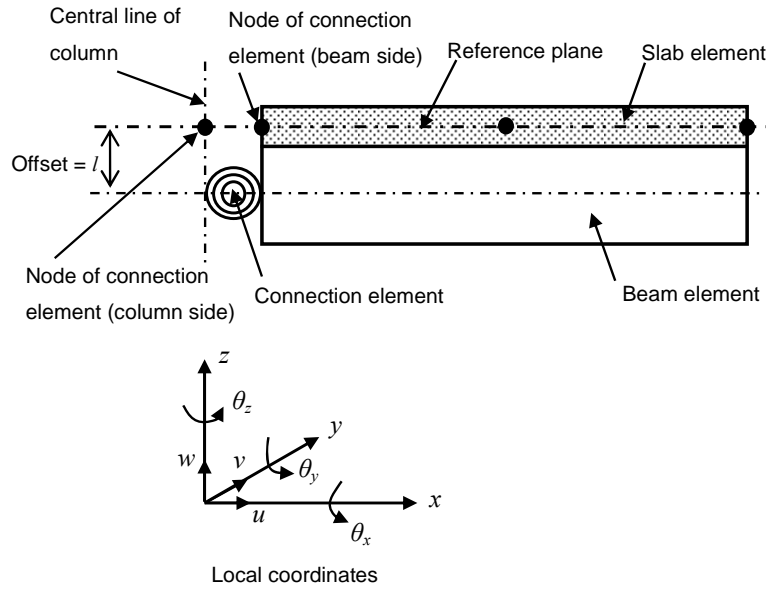


Fig. 2 Two-noded connection element

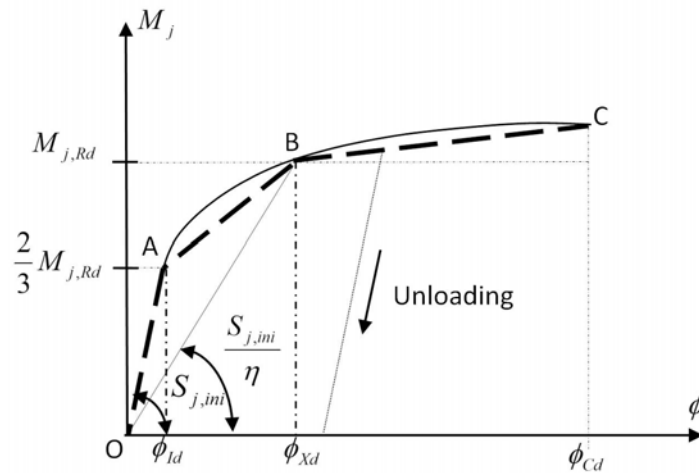


Fig. 3 Tri-linear moment-rotation characteristic used for the connection element

mainly six stiffness coefficients which are needed to be determined in the stiffness matrix.

In this paper only the in-plane behaviour of the connection element is considered. One of the main objectives of this study is to develop a numerical procedure for determining the bending moment characteristic of the end-plate connection in fire. The moment-rotation characteristic of the connection element is represented as a tri-linear curve as shown in Fig. 3. In the figure, the initial rotational stiffness of the connection  $S_{j,ini}$  is calculated based on the formulas proposed in Eurocode 3 Part 1.8 (2005b). It is determined according to a combination of stiffness coefficients of several basic joint components. The details can be found in the Reference (Huang 2011). In this study a new model is developed to calculate the moment resistance  $M_{j,Rd}$  for the end-plate

connection at elevated temperatures where the moment-rotation curve of the connection is defined for each temperature level. Based on the moment-rotation curve shown in Fig. 3 the rotational stiffness coefficient  $k_{55}$  in the connection element stiffness matrix  $\mathbf{K}$  is defined. The details for determining axial stiffness coefficient  $k_{11}$ , vertical shear stiffness coefficient  $k_{33}$ , stiffness coefficients related to the out-of-plane degrees of freedom  $k_{22}$ ,  $k_{44}$  and  $k_{66}$  can be found in the Reference (Huang 2011).

In the model proposed in this paper, the numerical procedure for determining the tension, compression and moment resistances of the end-plate connection is based on the component-based method. The connection is divided into tension and compression zones.

### 2.1 The tension resistance of the connection

The main components in the bolted end-plate connection can be represented using equivalent T-stubs, as shown in Fig. 4, which have been traditionally applied to represent the components in the tension zone. As shown in Fig. 5, there are three different failure modes for a T-stub assembly. It can be seen that in Section 2.1.1, a first plastic hinge is formed at the flange-to-web intersection, then followed by the yielding and fracture of the bolts. In Section 2.1.2, the T-stub flange suffers complete yielding, which has a first plastic hinge occurring in the middle and a second plastic hinge forming in the bolt line. In Section 2.1.3, however, the T-stub flange remains elastic but fails due to the fracture of the bolts. These three failure mechanisms should therefore be considered in the proposed model.

A simplified analytical model has been developed by Spyrou *et al.* (2004) to calculate the tension resistance of individual T-stub. The model is derived from elastic beam theory, and a multi-linear representation is used to describe the relationship between tension resistance of the

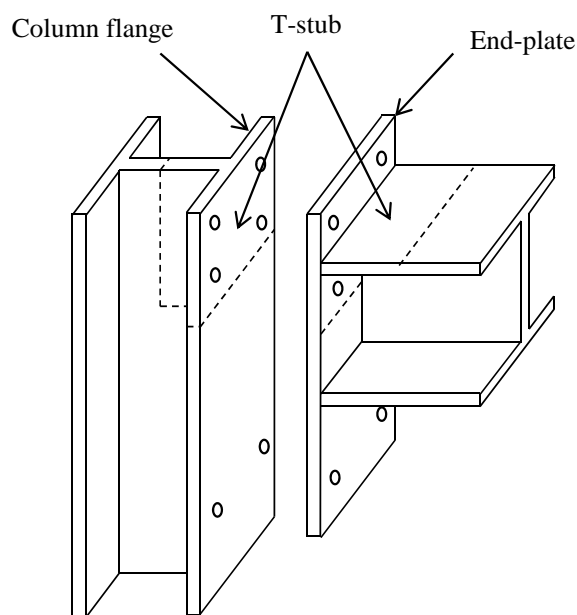


Fig. 4 T-stubs configuration of end-plate connection

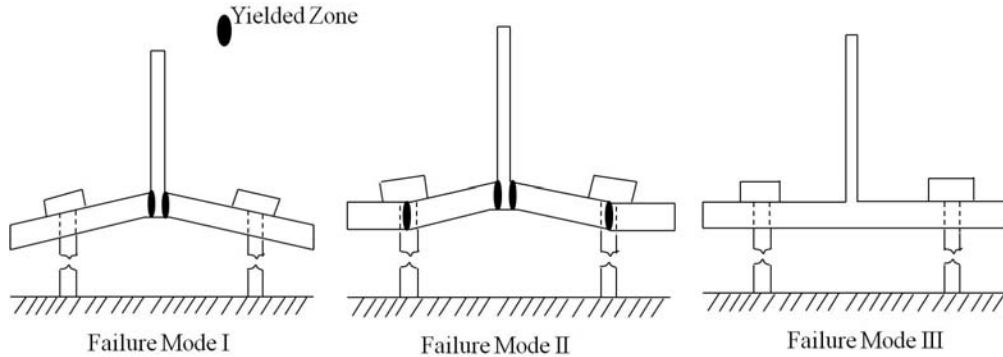


Fig. 5 Three failure mechanisms of a T-stub

T-stub and the deformation of the T-stub and bolts. However, the failure criterion hasn't been developed in his model, so the model cannot be directly adapted to calculate the tension capacity of the connection. Hence, in this paper, based on the Spyrou's model, three proper displacement failure criteria are proposed for the three failure modes of a T-stub to capture its tension resistance at elevated temperatures. In the current model, based on the tension capacity of the T-stub of each bolt row, the resistances of tension and bending of the connection are calculated.

### 2.1.1 Failure Mode I

As can be seen from Fig. 5, in Failure Mode I, bolts start to yield after the formation of the first plastic hinge, and then fracture before further yielding of the T-stub. In this case, a tri-linear curve is employed to determine the relationship between the tension force and the displacement of the T-stub as shown in Fig. 6(a). In order to define the tri-linear curve, three points  $(\delta_{cl,pl}, F_{cl,pl})$ ,  $(\delta_{cl,pl}^I, F_{cl,pl}^I)$  and  $(\delta_{t,1,Rd}, F_{t,1,Rd})$  need to be defined. At the first point  $F_{cl,pl}$  and  $\delta_{cl,pl}$  are the force and displacement at the T-stub flange respectively, when the first plastic hinge forms at the flange-to-web intersection (see Fig. 5). Using classical beam theory they are calculated when the maximum bending moment exceeds the plastic moment resistance of the T-stub. At the second point  $F_{cl,pl}^I$  and  $\delta_{cl,pl}^I$  are the T-stub force and related displacement, when bolts start to yield after the formation of the first plastic hinge. At this stage, part of the T-stub still remains elastic. By applying the same analysis theory, the displacement  $\delta_{cl,pl}^I$  could be given as a linear function relating to the T-stub force  $F_{cl,pl}^I$ . After the yielding of bolts, the increment of T-stub force is all taken by the bolts until they fracture. Therefore at the third point  $F_{t,1,Rd}$  is the ultimate tension resistance of the T-stub when bolts fracture, and  $\delta_{t,1,Rd}$  is the related total deflection. The magnitude of these six parameters is dependent on the geometry and material properties of the T-stub considered. The detail formulations for calculating them can be found in the Reference (Spyrou *et al.* 2004).

### 2.1.2 Failure Mode II

The main difference between Failure Mode II and Failure Mode I is that in Failure Mode II, after the formation of the first plastic hinge, instead of bolts starting to yield, a second plastic hinge forms at the bolt axis (see Fig. 5). Hence multi-linear curve is used to represent the relationship between the tension force and the displacement of the T-stub. As shown in Fig. 6(b),

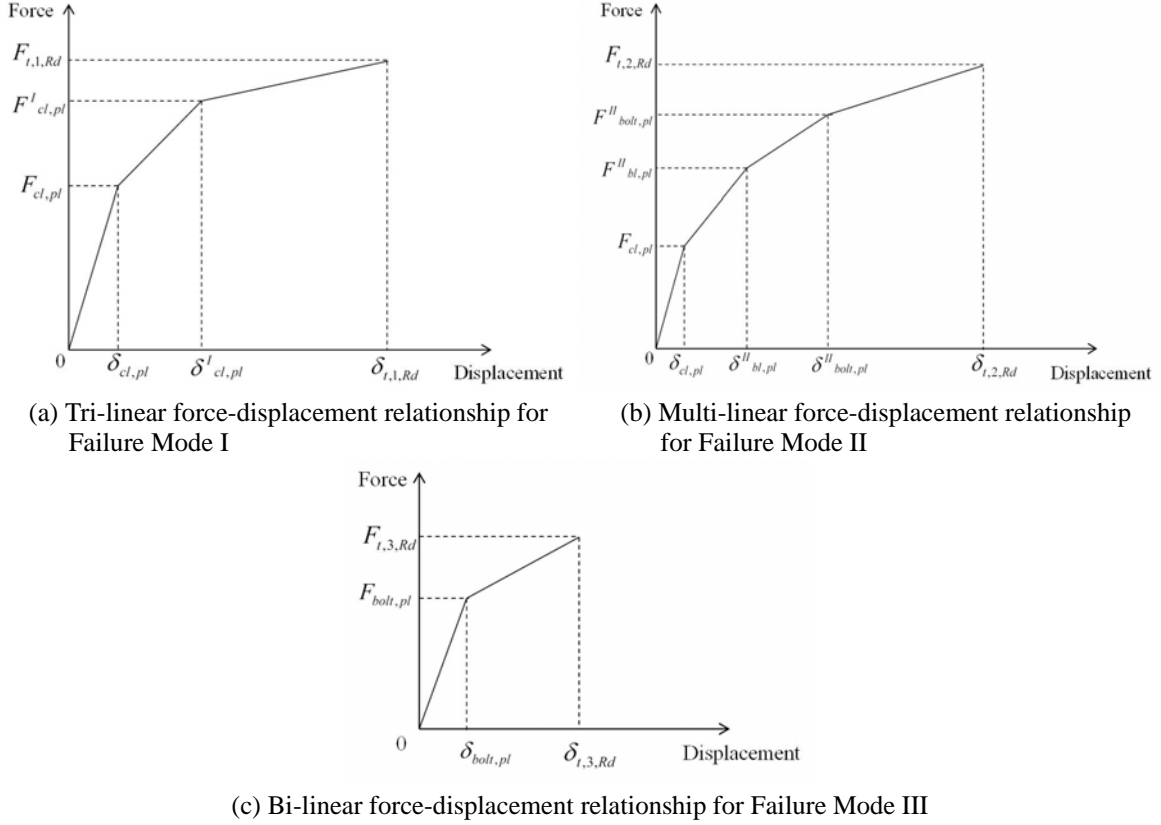


Fig. 6 Multi-linear force-displacement relationships for Failure Mode I, II and III

there are four points  $(\delta_{cl,pl}, F_{cl,pl})$ ,  $(\delta^{II}_{bl,pl}, F^{II}_{bl,pl})$ ,  $(\delta^{II}_{bolt,pl}, F^{II}_{bolt,pl})$  and  $(\delta_{t,2,Rd}, F_{t,2,Rd})$  which need to be defined. At the first point  $F_{cl,pl}$  and  $\delta_{cl,pl}$  are the force and displacement of T-stub respectively when first plastic hinges forms, which are both same as those in Failure Mode I. At the second point  $F^{II}_{bl,pl}$  and  $\delta^{II}_{bl,pl}$  are the force and displacement when a second plastic hinge appears at the bolt line. After the formation of two plastic hinges, bolts take all the further force increment of the T-stub until they yield. At point 3  $F^{II}_{bolt,pl}$  and  $\delta^{II}_{bolt,pl}$  are the force and displacement of T-stub when bolts yield. And finally at point 4 the bolts fracture,  $F_{t,2,Rd}$  and  $\delta_{t,2,Rd}$  are the ultimate tension resistance and displacement of the T-stub. Again the value of these eight parameters is depended on the geometry and material properties of the T-stub considered. Reference (Spyrou *et al.* 2004) presents the detail formulations for calculating them.

### 2.1.3 Failure Mode III

Unlike the previous two failure modes, in Failure Mode III, the T-stub flange remains elastic, and it is the yielding of the bolts, and fractures that cause the failure. As shown in Fig. 6(c), a bilinear curve is adopted to represent the force-displacement relationship of the T-stub. There are two points  $(\delta_{bolt,pl}, F_{bolt,pl})$  and  $(\delta_{t,3,Rd}, F_{t,3,Rd})$  which need to be defined.  $F_{bolt,pl}$  and  $\delta_{bolt,pl}$  are the force and displacement of the T-stub due to the bolts yielding.  $F_{t,3,Rd}$  and  $\delta_{t,3,Rd}$  are the force and displacement when bolts fracture. The detail formulations for determining them can be found in

the Reference (Spyrou *et al.* 2004).

#### 2.1.4 Displacement failure criteria for three failure mode

In Spyrou's model (Spyrou *et al.* 2004), it is assumed that bolt fracture is the ultimate failure mode for all the three failure modes. However, the value of tension resistance when the bolt fracture is too high compared to the test results. Therefore, it is necessary to develop reasonable failure criteria to identify the tension resistance of T-stub at elevated temperatures. In this research, an intensive numerical parametric study has been conducted based on the test results of 45 T-stubs specimens with different geometry tested at elevated temperatures (Spyrou *et al.* 2004). Three displacement criteria are proposed for the different failure modes of T-stub. Using the displacement criteria the tension resistances of T-stub with different failure modes are determined. That is: the displacement criterion of Failure Mode I  $\delta_{cri,1} = 7$  mm; the displacement criterion of

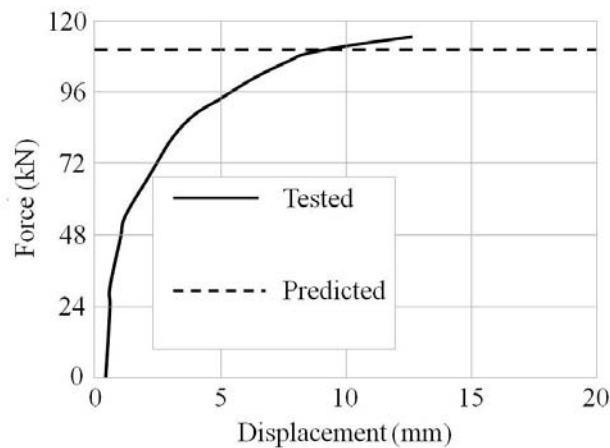


Fig. 7 Tension capacity predicted with applied displacement criteria (Test CA, 730°C, Spyrou *et al.* 2004)

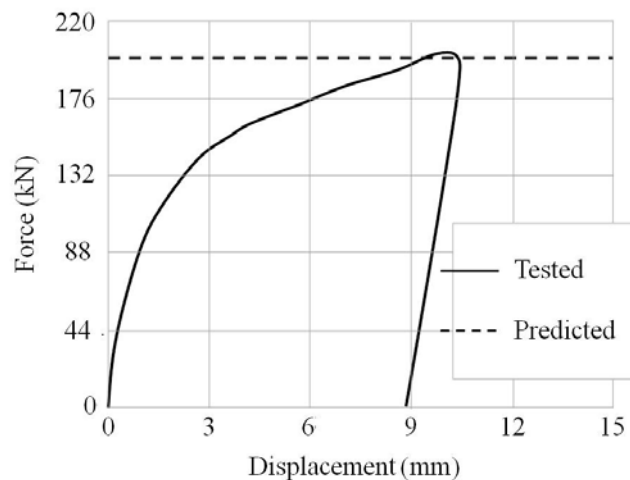


Fig. 8 Tension capacity predicted with applied displacement criteria (Test AC, 360°C, Spyrou *et al.* 2004)

Failure Mode II  $\delta_{cri,2} = 15$  mm; the displacement criterion of Failure Mode III  $\delta_{cri,3} = 3$  mm. The developed displacement criteria are then used to predict the tension resistances of 45 tested T-stubs, where good agreement with the test results was achieved. Here, two of the validation results are presented in Figs. 7 and 8, which are test CA at the temperature of 730°C and test AC at the temperature of 360°C. The dot line in the figures describes the tension resistance capacity determined by the current model. Based on the information collected from experiments, the failure mechanism of test CA at 730°C is Failure Mode I and the failure mode of test AC at 360°C is Failure Mode II which agreed with the predictions of the current model.

In the developed model, the final tension resistance of T-stub depends on the position of the displacement criteria within the multi-linear force-displacement curve. For Failure Mode I, the tension resistance of T-stub  $F_{t,1}$  is given as

$$F_{t,1} = \begin{cases} F_{cl,pl} & 0 < \delta_{cri,1} \leq \delta_{cl,pl} \\ F_{cl,pl} + (F_{cl,pl}^I - F_{cl,pl}) (\delta_{cri,1} - \delta_{cl,pl}) / (\delta_{cl,pl}^I - \delta_{cl,pl}) & \delta_{cl,pl} < \delta_{cri,1} \leq \delta_{cl,pl}^I \\ F_{cl,pl} + (F_{t,1,Rd} - F_{cl,pl}) (\delta_{cri,1} - \delta_{cl,pl}^I) / (\delta_{t,1,Rd} - \delta_{cl,pl}^I) & \delta_{cl,pl}^I < \delta_{cri,1} \leq \delta_{t,1,Rd} \\ F_{t,1,Rd} & \delta_{cri,1} > \delta_{t,1,Rd} \end{cases} \quad (4)$$

where  $\delta_{cri,1}$  is the displacement criterion of Failure Mode I.

For Failure Mode II, the tension resistance of T-stub  $F_{t,2}$  is calculated as

$$F_{t,2} = \begin{cases} F_{bl,pl}^{II} & 0 < \delta_{cri,2} \leq \delta_{bl,pl}^{II} \\ F_{bl,pl}^{II} + (F_{bolt,pl}^{II} - F_{bl,pl}^{II}) (\delta_{cri,2} - \delta_{bl,pl}^{II}) / (\delta_{bolt,pl}^{II} - \delta_{bl,pl}^{II}) & \delta_{bl,pl}^{II} < \delta_{cri,2} \leq \delta_{bolt,pl}^{II} \\ F_{bolt,pl}^{II} + (F_{t,2,Rd} - F_{bolt,pl}^{II}) (\delta_{cri,2} - \delta_{bolt,pl}^{II}) / (\delta_{t,2,Rd} - \delta_{bolt,pl}^{II}) & \delta_{bolt,pl}^{II} < \delta_{cri,2} \leq \delta_{t,2,Rd} \\ F_{t,2,Rd} & \delta_{cri,2} > \delta_{t,2,Rd} \end{cases} \quad (5)$$

where  $\delta_{cri,2}$  is the displacement criterion of Failure Mode II.

For Failure Mode III, the ultimate tension resistance of the T-stub  $F_{t,3}$  is determined as

$$F_{t,3} = \begin{cases} F_{bolt,pl} & 0 < \delta_{cri,3} \leq \delta_{bolt,pl} \\ F_{bolt,pl} + (F_{t,3,Rd} - F_{bolt,pl}) (\delta_{cri,3} - \delta_{bolt,pl}) / (\delta_{t,3,Rd} - \delta_{bolt,pl}) & \delta_{bolt,pl} < \delta_{cri,3} \leq \delta_{t,3,Rd} \\ F_{t,3,Rd} & \delta_{cri,3} > \delta_{t,3,Rd} \end{cases} \quad (6)$$

where  $\delta_{cri,3}$  is the displacement criterion of Failure Mode III.

### 2.1.5 Tension resistance of connection

In this model, the whole connection is considered as a combination of a column T-stub and an end-plate T-stub. Therefore, for each failure mode, the tension resistance is taken as the smaller value of two T-stub resistances. The final tension resistance of a single bolt row is determined as the minimum value of tension resistance of three failure modes. Hence, the final tension resistance of a single bolt row  $F_{tens,r,bolt}$  can be calculated as

$$F_{tens,r,bolt} = \min(F_{t,1,fc}; F_{t,1,ep}; F_{t,2,fc}; F_{t,2,ep}; F_{t,3,fc}; F_{t,3,ep}) \quad (7)$$

where  $F_{t,1,fc}$ ,  $F_{t,2,fc}$  and  $F_{t,3,fc}$  are the tension resistances of the column T-stub for Failure Mode I, Failure Mode II and Failure Mode III respectively,  $F_{t,1,ep}$ ,  $F_{t,2,ep}$  and  $F_{t,3,ep}$  are the tension resistances of the end-plate T-stub for Failure Mode I, Failure Mode II and Failure Mode III. The tension resistances of column T-stub and end-plate T-stub for three failure modes are determined by using Eqs. (4)-(6).

The tension resistance of the connection  $F_{tens}$  is given as follows

$$F_{tens} = \sum_{r=1}^N F_{tens,r,bolt} \quad (8)$$

where  $N$  is the total number of bolt rows in tension.

### 2.2 The compression resistance of the connection

The compression resistance of the whole connection  $F_{comp}$  is taken as the smaller value of the resistance of column web  $F_{c,cw}$  and the resistance of beam flange  $F_{c,bf}$ , that is

$$F_{comp} = \min(F_{c,cw}; F_{c,bf}) \quad (9)$$

$F_{c,bf}$  is calculated according to the Eurocode 3 Part 1.8 (2005). The calculation of  $F_{c,cw}$  is based on a simplified model developed by Block *et al.* (2007).

The force distribution in bolt rows is also considered in the model. The first condition that the effective tension resistance has to satisfy is

$$F_{et,Ed} \leq F_{comp} \quad (10)$$

$$F_{et,Ed} = \sum_{r=1}^N F_{tens,r,bolt} \quad (11)$$

where,  $N$  = total number of bolt rows in tension.

If  $F_{et,Ed} > F_{comp}$  the force distribution in bolt rows should be adopted to make sure that

$$F_{et,Ed} = \sum_{r=1}^N F_{tens,r,bolt} = F_{comp} \quad (12)$$

Normally the force will be reduced from the tension bolt row with the largest bolt row number (on the top of the connection).

### 2.3 The Bending moment resistance of the connection

The moment resistance  $M_{j,Rd}$  of a bolted end-plate connection may be calculated as

$$M_{j,Rd} = \sum_r h_r F_{tens,r,bolt} \quad (13)$$

where  $F_{tens,r,bolt}$  is effective tension resistance of bolt-row  $r$ ,  $h_r$  is distance from bolt-row  $r$  to the centre of compression,  $r$  is bolt-row number.

In order to consider the influence of axial force on the moment resistance of a connection the model proposed by Huang (2011) is adopted in this study.

In this paper steel material properties, such as yield strength; ultimate tensile strength and Young's module, are temperature dependent. Previous research indicates that the degradation of bolts' mechanical properties at elevated temperatures is much worse than the end-plate and the section of steel beam or column. However, the research conducted by Hu *et al.* (2009) indicated that the majorities of failure models of T-stabs are Mode I and Mode II. The influence of material degradation of the bolt by using different models on the final tension resistance of one bolt row is not very significant. Therefore for simplicity in this paper it is assumed that the material degradation of bolt at elevated temperatures is the same for the beam, column and end-plate – the model specified in Eurocode 3 Part 1.2 (2005a) is adopted.

### 3. Validations

The model presented above has been validated using a total of 22 end-plate connection tests. The validation includes 8 tests without the axial force at elevated temperatures, 12 tests subjected to axial force at both ambient and elevated temperatures and 2 fire tests of beam-to-column sub-frame. In this validation the tested material properties and measured temperature distribution within the connections were employed as input data for the modelling.

Fig. 9 presents the details of fire tests conducted by Leston-Jones (1997). All tests are consisted of a symmetric cruciform arrangement of a single  $152 \times 152 \times 23$  UC column 1.4 m high with two cantilever beams ( $254 \times 102 \times 22$  UB). The tests adopted a 12 mm thick end-plate with three M16-8.8 bolts. In all cases, the specimens were keeping at a constant load then gradually increased the temperature, which reflected the real situation in building fire. Four different loads were applied to the connection during the tests, which were 5 kNm, 10 kNm, 15 kNm and 20 kNm to

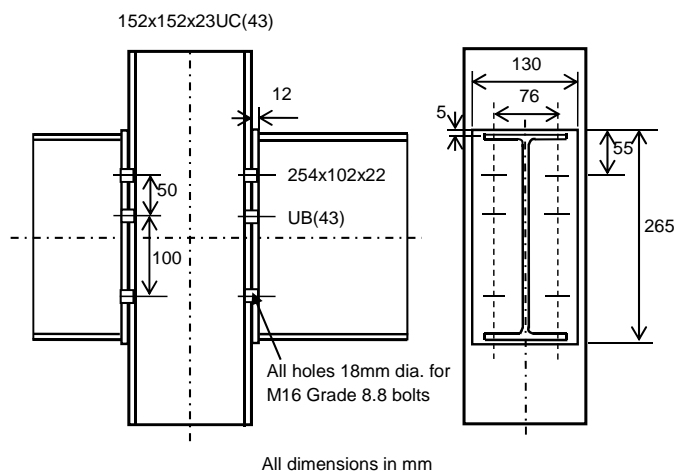


Fig. 9 Details of test specimens used by Leston-Jones (1997)

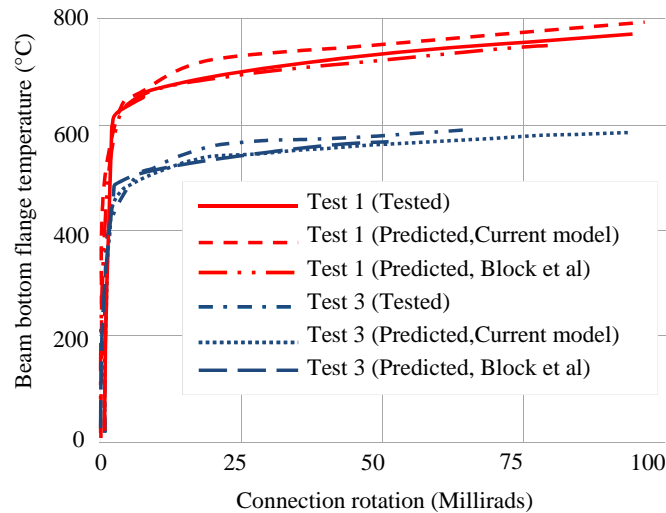


Fig. 10 Comparison of predicted and measured connection rotations at elevated temperatures for Test 1 and Test 3 (Leston-Jones 1997)

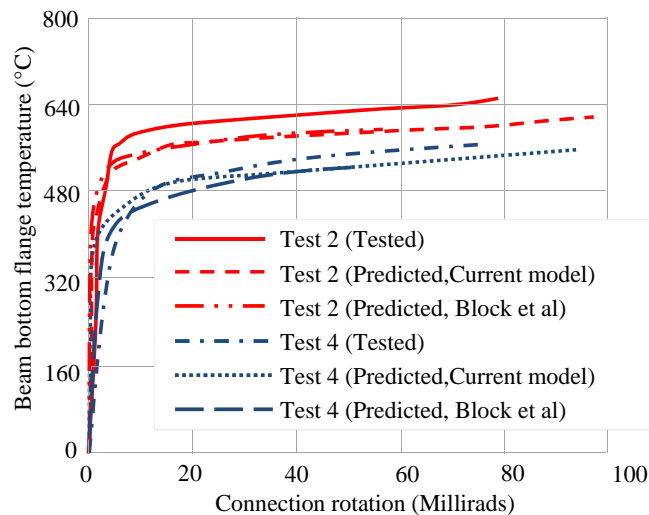


Fig. 11 Comparison of predicted and measured connection rotations at elevated temperatures for Test 2 and Test 4 (Leston-Jones 1997)

Test 1, Test 2, Test 3 and Test 4 respectively. The comparison results are illustrated in Figs. 10 and 11, together with the predictions by the component model (Block *et al.* 2007). It is evident that the predictions of the current model agree well with the experimental data and the component model's predictions.

Another four tests without axial force at elevated temperature utilized for validation were conducted by Al-Jabri (1999). The tests details are given in Fig. 12. A cruciform arrangement was chosen for the tests, consisting of two  $356 \times 171 \times 51$  UB beams 1.9 m long symmetrically

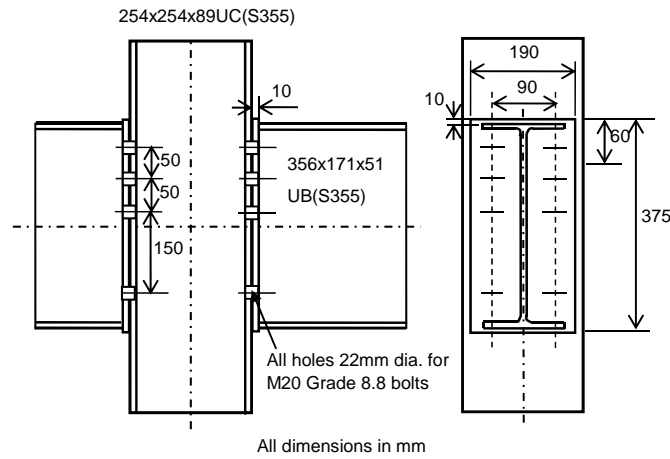


Fig. 12 Details of test specimens used by Al-Jabri *et al.* (2005)

connected to a  $254 \times 254 \times 89$  UC column 2.7 m high. The thickness of endplate adopted was 10 mm. Eight M20 Grade 8.8 bolts were used. All these tests were conducted under a constant load and then the temperature was increased gradually. Four different load levels were applied to the same connection, which were 27.4 kNm, 54.8 kNm, 82.1 kNm and 110 kNm to Test 1, Test 2, Test 3 and Test 4 respectively. The comparison results are given in Figs. 13 and 14. It is evident that the proposed analytical model agrees well with the experimental data. These comparison results

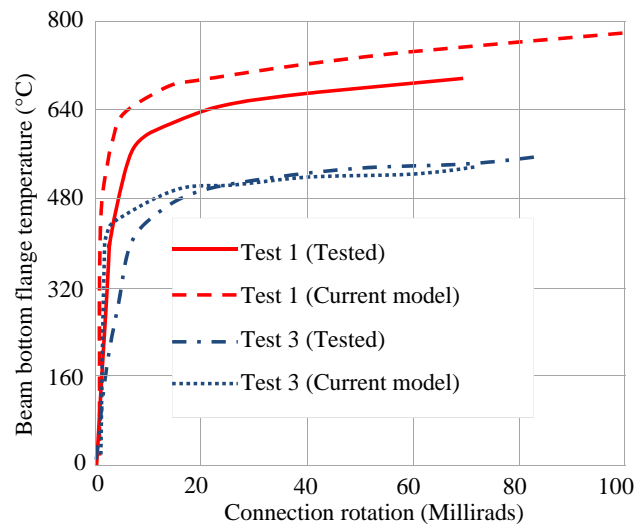


Fig. 13 Comparison of predicted and measured connection rotations at elevated temperatures for Test 1 and Test 3 (Al-Jabri *et al.* 2005)

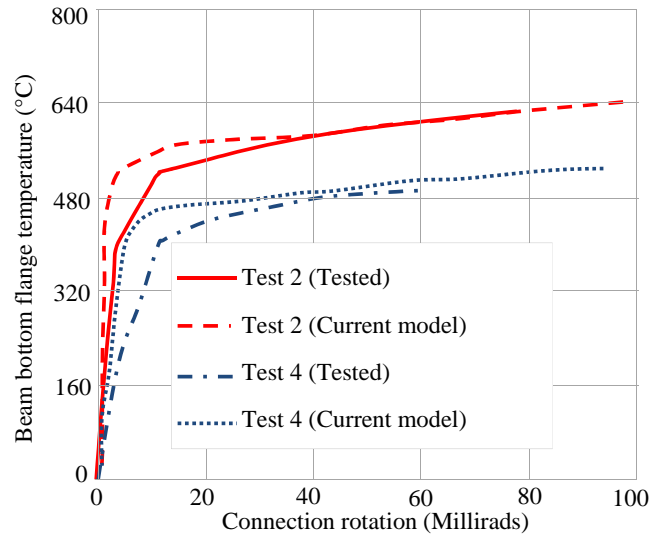


Fig. 14 Comparison of predicted and measured connection rotations at elevated temperatures for Test 2 and Test 4 (Al-Jabri *et al.* 2005)

demonstrate that the new model has the ability to accurately predict the behaviour of connections without axial force at elevated temperatures.

The 12 tests with the axial force acting on the connections were conducted by Yu *et al.* (2009) at the University of Sheffield. The details of the test specimens are given in Fig. 15. The connections are comprised of a  $305 \times 165 \times 40$  UB beam connected to a  $254 \times 254 \times 89$  UC column with three M20 Grade 8.8 bolts. The thickness of end-plate was 10 mm in the eleven tests, except for the test EP\_550\_35\_11-12-07\_8 mm, which adopted the end-plate with 8 mm thickness. The tests were conducted by heating the specimen to the specified temperature then increasing the load until failure. The force was applied with inclined angle ( $\theta$ ) to the axis of the connected beam. A total of three angles were employed,  $\theta = 35^\circ, 45^\circ, 55^\circ$ . These three different angles represent three

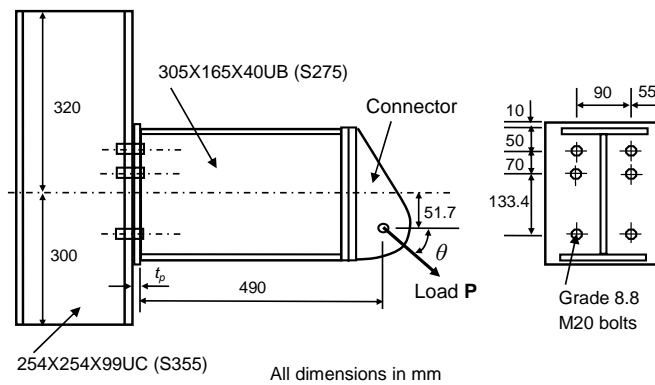


Fig. 15 Details of test specimens used by Yu *et al.* (2009)

different combinations of shear and tying forces. The comparisons for two ambient tests with different angles are displayed in Fig. 16. Figs. 17-21 show the comparison results for the rest of 10 tests at elevated temperatures. It can be clearly seen that the predicted results by the current model correlate well with the tests data. In the figures the unloading path of the connections is correctly predicted by the current model (see the straight lines with the slopes equal to initial stiffness of the

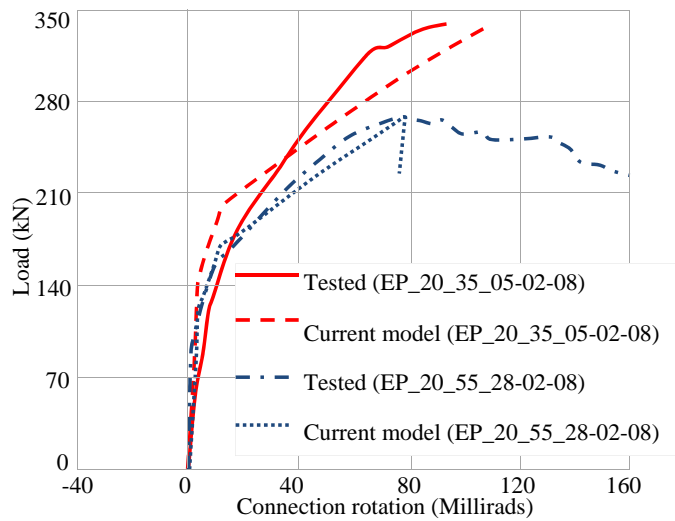


Fig. 16 Comparison of predicted and measured connection rotations at ambient temperature for Sheffield's tests: EP\_20\_35\_05-02-08 ( $\theta = 35^\circ$ ) and EP\_20\_55\_28-02-08 ( $\theta = 55^\circ$ ) (Yu *et al.* 2009)

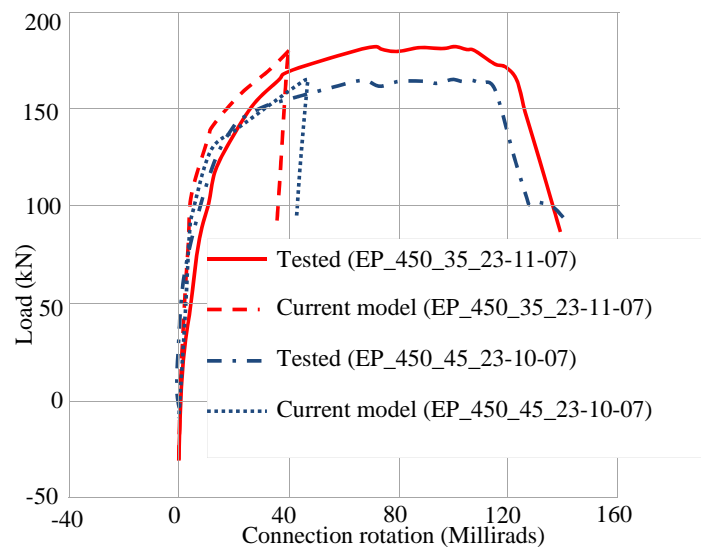


Fig. 17 Comparison of predicted and measured connection rotations at 450°C for Sheffield's tests: EP\_450\_35\_23-11-07 ( $\theta = 35^\circ$ ) and EP\_450\_45\_23-10-07 ( $\theta = 45^\circ$ ) (Yu *et al.* 2009)

connection). However, for the test results the descending part of the curves represents an unstable failure process of the connections.

Finally, two fire tests on a beam-to-column sub-frame conducted at the University of Coimbra (Santiago 2008) are employed to validate this model. The tests details are shown in Fig. 22. This sub-frame is consisted of an unprotected IPE300 cross-section beam with 5.7 m free span

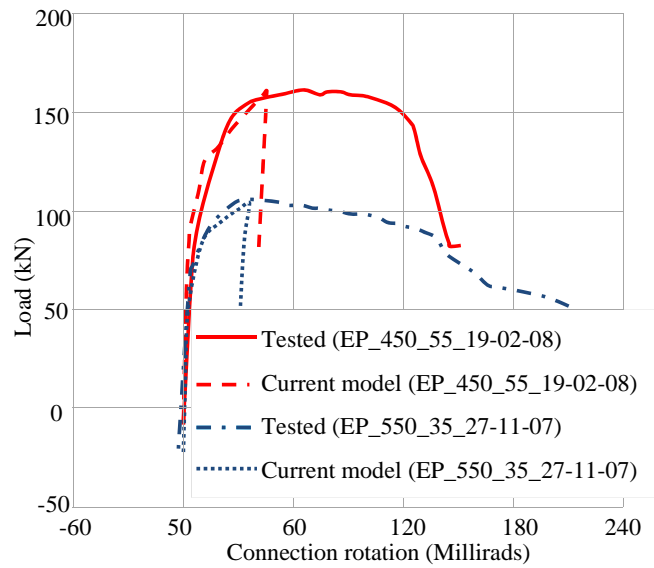


Fig. 18 Comparison of predicted and measured connection rotations for Sheffield's tests: EP\_450\_55\_19-02-08 (450°C,  $\theta = 55^\circ$ ) and EP\_550\_35\_27-11-07 (550°C,  $\theta = 35^\circ$ ) (Yu *et al.* 2009)

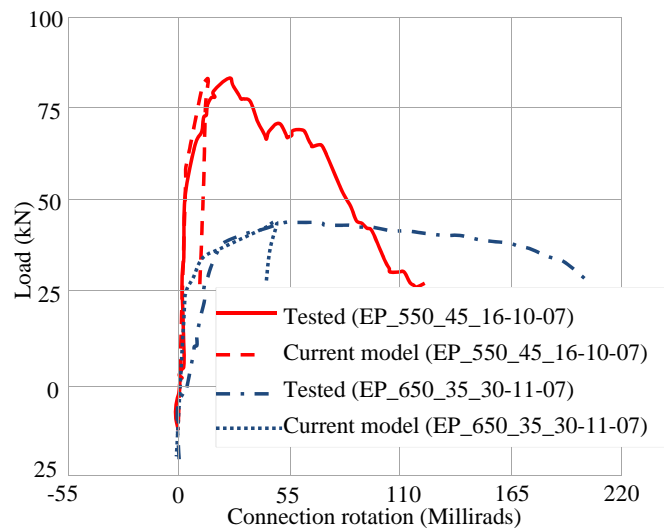


Fig. 19 Comparison of predicted and measured connection rotations for Sheffield's tests: EP\_550\_45\_16-10-07 (550°C,  $\theta = 45^\circ$ ) and EP\_650\_35\_30-11-07 (650°C,  $\theta = 35^\circ$ ) (Yu *et al.* 2009)

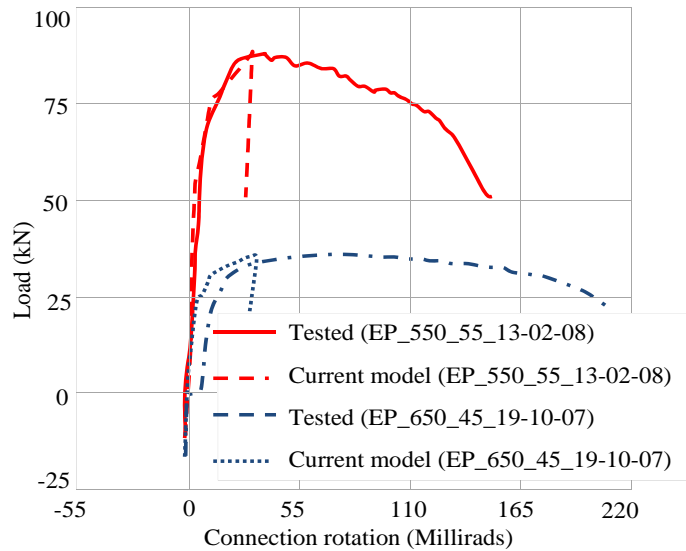


Fig. 20 Comparison of predicted and measured connection rotations for Sheffield's tests: EP\_550\_55\_13-02-08 (550°C,  $\theta = 55^\circ$ ) and EP\_650\_45\_19-10-07 (650°C,  $\theta = 45^\circ$ ) (Yu *et al.* 2009)

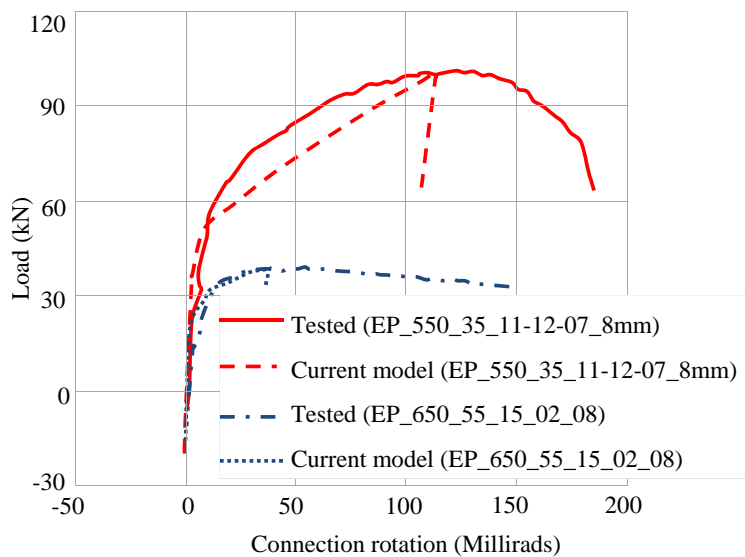


Fig. 21 Comparison of predicted and measured connection rotations for Sheffield's tests: EP\_550\_35\_11-12-07\_8 mm (550°C,  $\theta = 35^\circ$ ) and EP\_650\_55\_15\_02\_08 (650°C,  $\theta = 55^\circ$ ) (Yu *et al.* 2009)

connected to two thermally insulated HEA300 cross-section columns. A natural fire was applied to this sub-frame, which including the heating and cooling phases. The behaviour of two connections EJ01 and FJ03 in the tests were investigated. EJ01 is an extended end-plate connection adopting three M20 Grade 8.8 bolts while FJ03 is a flush end-plate connection with two M20 Grade 8.8 bolts. For test EJ01 the maximum beam temperature of 898°C was reached at about 50 min then

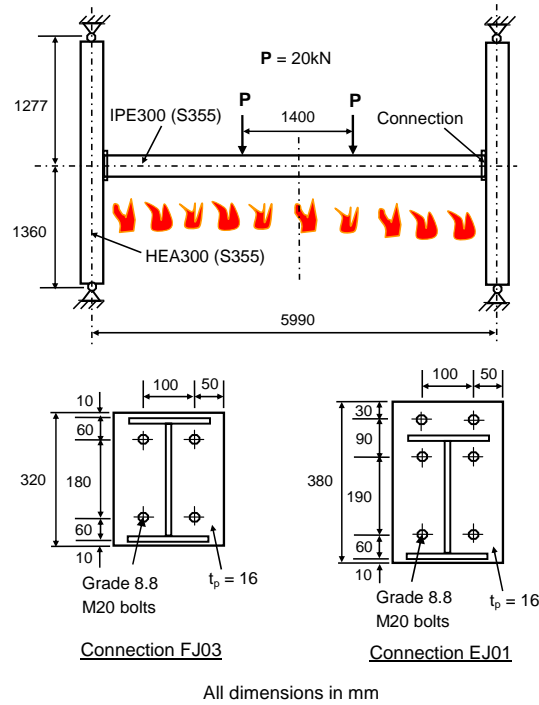


Fig. 22 Test details of a beam-to-column substructure (Santiago 2008)

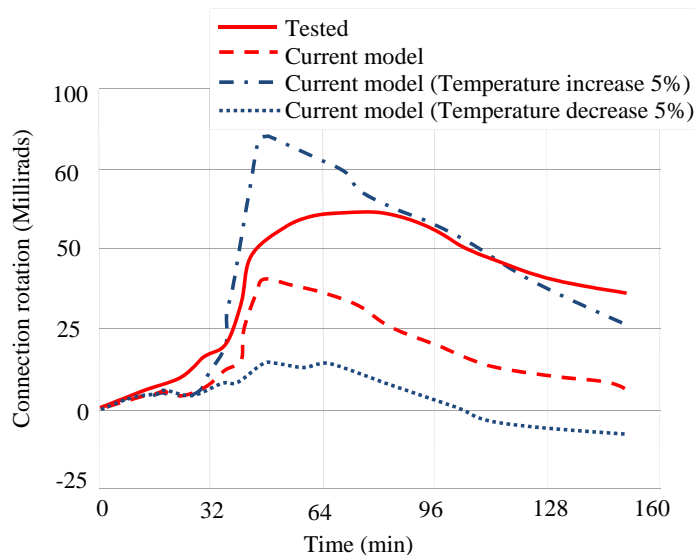


Fig. 23 Comparison of predicted and measured connection rotations for test EJ01 (Santiago 2008)

cooled down to about 180°C at 150 min. For test FJ03 the maximum beam temperature of 900°C was reached at about 40 min and kept almost constant until 50 min then cooled down to about 200°C at 150 min. All tested material properties and temperatures of unprotected beam,

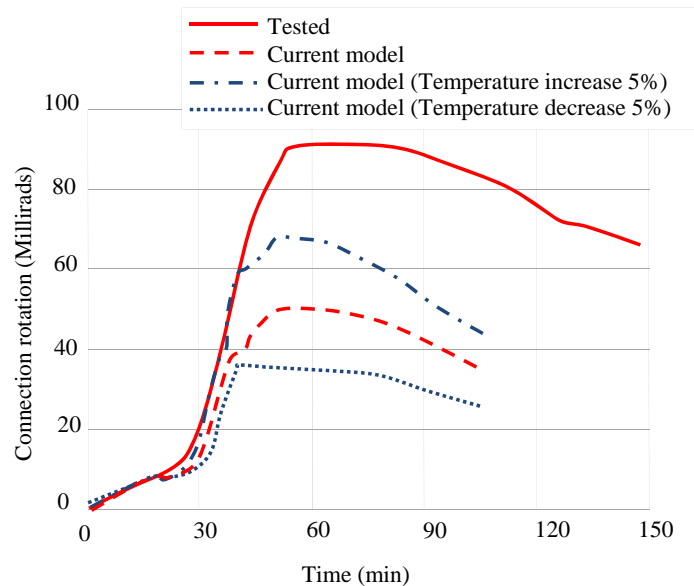


Fig. 24 Comparison of predicted and measured connection rotations for test FJ03 (Santiago 2008)

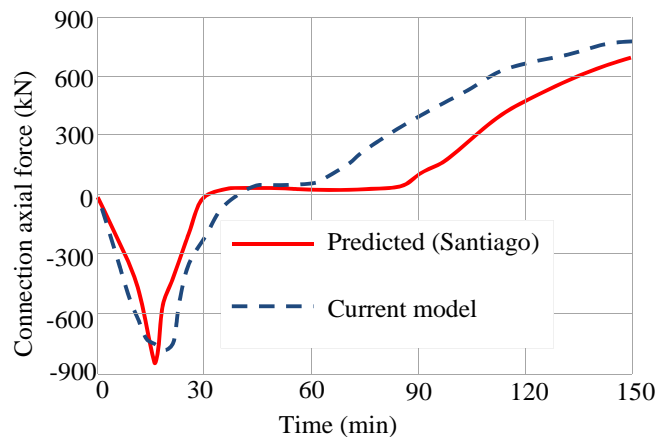


Fig. 25 Comparison of predicted axial forces at the connection for test EJ01 (Santiago 2008)

connections and protected columns were used as input for the modelling.

Figs. 23 and 24 show the comparisons of the predicted and tested rotations for the tests EJ01 and FJ03. It is noted that the predicted rotations are significant lower than tested data. This is due to a lack of details for the tested temperature distributions within the connections. In the modelling the connections' temperatures were assumed as uniform and equalled to average tested temperatures. Therefore, connections' temperatures used in the modelling may significant lower than real tested temperatures within the connections. In order to investigate the influence of temperatures on the behaviour of the connections two tests (EJ01 and FJ03) are modelled again with two different temperature patterns. The first temperature pattern is to increase the connections' temperature by 5% of the original temperatures. The second temperature pattern is to

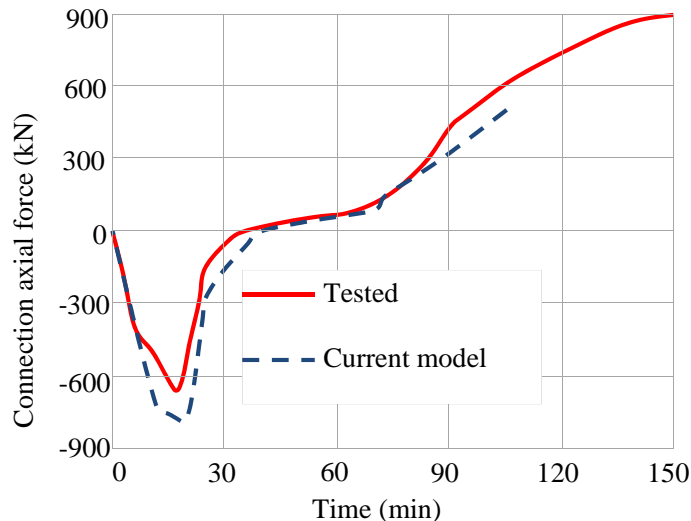


Fig. 26 Comparison of predicted and measured axial forces at the connection for test FJ03 (Santiago 2008)

reduce the connections' temperature by 5% of the original temperatures. The predictions by using those two temperature's patterns are also shown in Figs. 23 and 24. It can be clearly seen that the rotations of the connections are very sensitive to the small temperature variations. The predicted axial force acting on the connection EJ01 predicted by current model is shown in Fig. 25 together with the predictions by Santiago (2008) in which the detail 3D finite element approach was used. It is clear that good agreement was achieved. Fig. 26 shows the comparison of tested and predicted axial force acting on the connection FJ03. It can be seen that the predictions of the current model are in very good agreement with the test data.

#### 4. Conclusions

In this paper a robust 2-noded connection element has been developed for modelling the bolted end-plate connection between steel beam and column at elevated temperatures. The developments are based on the model proposed by Huang (2011) and incorporated with the works done by Spyrou *et al.* (2004) and Block *et al.* (2007) to more precisely determinate the tension, compression and bending moment capacities of end-plate connection in fire. Hence, in this model the connection failure due to bending, axial tension and compression are considered. Also the influence of axial tensile force of the connected beam on the connection is taken into account. The model has the advantages of both the simple and component-based models. In order to validate the model a total of 22 experimental tests are used. It is obvious that this new connection model has the ability to accurately predict the behaviour of the end-plate connections at elevated temperatures. It is evident that the influence of temperature on the behaviour of the connections is significant. We conclude from the validation data that the model can be used to represent the end-plate connections in performance-based fire resistance design of steel-framed composite buildings.

## Acknowledgements

We would like to thank Brunel University for funding this Ph.D. research.

## References

- Al-Jabri, K.S., Burgess, I.W., Lennon T. and Plank, R.J. (2005), "Moment-rotation-temperature curves for semi-rigid joints", *J. Constr. Steel Res.*, **61**(3), 281-303.
- Al-Jabri, K.S. (1999), "The behaviour of steel and composite beam-to-column connections in fire", Ph.D. Dissertation, University of Sheffield, Sheffield, UK.
- Block, F.M., Davison, J.B., Burgess, I.W. and Plank, R.J. (2007), "The development of a component-based connection element for endplate connections in fire", *Fire Safety J.*, **42**(6-7), 498-506.
- European Committee for Standardization CEN (2005a), Eurocode 3: Design of steel structures: Part 1.2: General rules-structural fire design, BS EN 1993-1-2, British Standards Institution.
- European Committee for Standardization CEN (2005b), BS EN 1993-1-8, Eurocode 3: Design of steel structures, Part 1.8: Design of joints, British Standards Institution.
- Hu, Y., Davison, J.B., Burgess, I.W. and Plank, R.J. (2009), "Component modelling of flexible end-plate connections in fire", *Int. J. Steel Struct.*, **9**(1), 1-15.
- Huang, Z. (2011), "A connection element for modelling end-plate connections in fire", *J. Constr. Steel Res.*, **67**(5), 841-853.
- Lawson, R.M. (1990), "Behaviour of steel beam-to-column connections in fire", *Struct. Eng.*, **68**(14), 263-271.
- Leston-Jones, L.C. (1997), "The influence of semi-rigid connections on the performance of steel framed structures in fire", Ph.D. Dissertation, University of Sheffield, Sheffield, UK.
- Qian, Z.H., Tan, K.H. and Burgess I.W. (2009), "Numerical and analytical investigations of steel beam-to-column joints at elevated temperatures", *J. Constr. Steel Res.*, **65**(5), 1043-1054.
- Ramli Sulong, N.H., Elghazouli, A.Y., Izzuddin, B.A. and Ajit, N. (2010), "Modelling of beam-to-column connections at elevated temperature using the component method", *Steel Comp. Struct., Int. J.*, **10**(1), 23-43.
- Santiago, A. (2008), "Behaviour of beam-to-column steel joints under natural fire", Ph.D. Dissertation, University of Coimbra, Coimbra, Portugal.
- Spyrou, S., Davison J., Burgess I.W. and Plank R.J. (2004), "Experimental and analytical investigation of the 'tension zone' component within a steel joint at elevated temperatures", *J. Constr. Steel Res.*, **60**(6), 867-896.
- Yu, H., Burgess, I.W., Davison, J.B. and Plank, R.J. (2009), "Experimental investigation of the behaviour of fin plate connections in fire", *J. Constr. Steel Res.*, **65**(3), 723-736.
- Zoetemeijer, P. (1974), "A design method for the tension side of statically loaded, bolted beam-to-column connections", *HERON*, **20**(1), 1-59.